IEEE Access
Multidisciplinary | Rapid Review | Open Access Journal

Received January 27, 2018, accepted February 24, 2018, date of publication March 5, 2018, date of current version June 5, 2018.

*Digital Object Identifier 10.1109/ACCESS.2018.2812187*

# Real-Time SOSM Super-Twisting Combined With Block Control for Regulating Induction Motor Velocity

**ONOFRE A. MORFIN[1], FREDY ALBERTO VALENZUELA[2], REYMUNDO RAMÍREZ BETANCOUR[2], CARLOS EDUARDO CASTAÑEDA[3], RIEMANN RUÍZ-CRUZ[4], (Member, IEEE), AND ANTONIO VALDERRABANO-GONZALEZ[5]**

[1]Departamento de Eléctrica y Computación, Instituto de Ingeniería y Tecnología, Universidad Autónoma de Ciudad Juárez, Ciudad Juárez 32310, México
[2]División Académica de Ingeniería y Arquitectura, Universidad Juárez Autónoma de Tabasco, Villahermosa 86040, México
[3]Centro Universitario de los Lagos, Universidad de Guadalajara, Lagos de Moreno 47460, México
[4]Instituto Tecnológico y Estudios Superiores de Occidente , Tlaquepaque 45604, México
[5]Facultad de Ingeniería, Universidad Panamericana, Zapopan 45615, México

Corresponding author: Carlos Eduardo Castañeda (ccastaneda@lagos.udg.mx)

This work was supported by the Departamento de Eléctrica y Computación del Instituto de Ingeniería y Tecnología de la Universidad Autónoma de Ciudad Juárez (México), Programa para el Desarrollo Profesional Docente under Grant PROMEP/103.5/11/901 Folio UACJ/EXB/155 and in part by the Consejo Nacional de Ciencia y Tecnología (México) by the retention program under Grant 120489.

**ABSTRACT** On this paper, a robust velocity controller applied to a three-phase squirrel-cage induction motor under variable load conditions is designed. The induction motor drives an induction generator representing the load which freely delivers the generated power to the utility grid. The closed-loop scheme is designed at $\alpha\beta$ coordinate frame and is based on the linearization block control technique in combination with the super-twisting algorithm. The controlled output variables are the angular mechanical velocity and the square modulus of rotor flux linkages. The motor reference velocity is set up by a pulse train above the synchronous velocity and, consequently, the impelled induction machine operates in generator mode; meanwhile, the reference of rotor flux square modulus varies according to load condition of the induction motor. In order to estimate the non-measurable variables, both a rotor flux linkages observer and a load torque observer are designed. For the first one, a non-linear state observer using first order sliding modes is applied at $\alpha\beta$ coordinate frame and, for the second one, a Luenberger reduced asymptotic observer is used. The validation of the robustness for the proposed velocity controller is performed in a real-time experiment using a work-bench.

**INDEX TERMS** Block control, induction motor, sliding mode observer, super-twisting.

## I. INTRODUCTION

The sliding modes (SM) is a type of variable structure control system (VSCS) and is characterized by its low sensitivity to external disturbances and parameter variations in the plant [1], [2]. By applying the sliding mode control technique, the closed-loop system order is reduced because the sliding variable, as control argument, is defined by the system states; consequently, the plant parameter amount is reduced, thus eliminating the necessity of knowing all system parameters exactly [1], [2]. The drawback of sliding modes is the chattering effect presented as noise in output variables due to the switching at high frequency of the control signal and the non-modeled fast dynamics of the actuators and sensors [1]. A good choice to avoid the chattering effect is the application of the super-twisting control law, which is a second order sliding mode technique [3]. The super-twisting algorithm can be applied to a system where the control signal appears in the first time derivative of the sliding variable; it provides finite time convergence to the origin for the sliding variable and its time derivative simultaneously. Additionally, this control law sets a continuous control signal and, consequently, the chattering effect is reduced [3]–[5].

The electric machines model has an ideal structure to design the sliding variable and apply the sliding mode control, as is the case of the squirrel-cage induction motor. This motor has the simplest structure, and is the most rugged of all AC machines [15]. However, its mathematical model is a complex system with some time-varying parameters.

Many works have been reported about the topic of induction motor control, where the electrical variables are referred to a new coordinate frame [6]. The field-oriented control is one of the most commonly applied, where output variables such as electromagnetic-torque/angular-velocity and rotor flux square modulus are decoupled by means of the choice of either the stator flux or the rotor flux as reference frame [7]–[12]; nevertheless, this procedure requires an exact knowledge of the model. Other authors propose to control the velocity and square modulus of the rotor flux linkages referring the electrical variables on $\alpha\beta$ coordinate frame which is fixed on the stator [13]. But these authors set a constant reference value of the rotor flux square modulus and do not consider the load condition variations; whereas in [14], the authors propose a reference function to rotor flux that varies minimizing the internal losses. However, their calculation is complex and requires a huge computational effort. A main condition of the real-time implementation for the induction motor controller is the knowledge of all state variables. However, the rotor flux leakages usually cannot be measured; thus, it is necessary to estimate its value. Some works have been reported with different techniques for the rotor flux linkages observer design, within which the robust observers for rotor flux applying sliding modes stand out. These observers include a discontinuous input that makes the estimation error between the output vector and its value estimated vanishes to zero [7], [16], [17].

In this paper, a robust velocity controller applied to a squirrel-cage induction motor is proposed. This controller combines the block control linearization technique with the second-order sliding-modes (SOSM) super-twisting control law, in order to set a robust closed-loop system. The main advantage of this velocity controller is its symplicity due to is only neccesary to calculate a surface through stator currents and apply a first order control law, avoiding the complexity of the induction motor model. Additionally, the controller proposed reduces the chattering effect, respect to conventional sliding modes, due to the super-twisting control law is a continuous signal. The major contribution of this controller is the ability to operate under variable load conditions, where the reference function of the rotor flux square modulus varies according to the stator current variations due to changes in the mechanical load. The load is represented by a coupled induction generator which freely delivers the generated power to the utility grid when it operates above synchronous velocity. The validation of the proposed controller is performed through a real-time test in a work-bench, under two simultaneous external disturbances: a pulse train signal above synchronous velocity as a reference signal, and consequently, a pulse train of variations on the load torque through a coupled induction generator. It can be commented that the proposed algorithm for controlling the mechanical velocity of the induction motor is robust, practical and simple, and it can be used as basis for further applications on artificial intelligence techniques such as: adaptive fuzzy tracking control, adaptive neural control, adaptive control by combining backstepping technique with neuronal network, observed based fuzzy output-feedback control, among others [24]–[27].

This paper is organized as follows: in section II, the mathematical model of the squirrel-cage induction motor is presented; section III presents the feedback linearization technique by block control; in section IV, the super-twisting algorithm as a second order slide mode technique is described; section V introduces two state observers to estimate the rotor flux linkages and load torque; section VI shows real-time experimental results with velocity tracking of a pulse train, in order to validate the robustness of the proposed controller; conclusions and some remarks about the application of slinding modes on induction motors are presented in section VII.

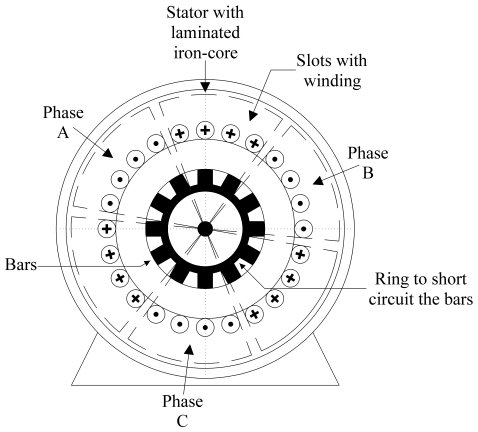


**FIGURE 1.** Induction motor scheme.

## II. SQUIRREL-CAGE INDUCTION MOTOR MODEL

The squirrel-cage induction motor is a rugged electromechanical device which is very reliable, low priced, and almost maintenance free; thus it is extensively used in industry. A three-phase induction motor has a uniform air-gap and it is provided with a distributed winding that is mounted at slots on the inner surface of the stator. The stator winding has a symmetric structure and it is electrically balanced. On the other hand, the rotor winding is electrically balanced and is electromagnetically induced. This winding consists of silicon steel laminations with slots at the external surface with aluminum bars that are embedded in the rotor slots and shorted at both ends by aluminum end rings [15], see Fig. 1.

It is common practice to assume that the flux linkages-current relation ($\lambda - i$) is linear when the induction motor model is set up, due to the air-gap presence. Even more, the model is complex on the *abc* coordinate system because the mutual inductances between the stator winding and the rotor winding, change periodically with time [6]. In order to simplify the model, the Clarke transformation matrix is traditionally applied to refer the electric variables from *abc* system to $\alpha\beta 0$ coordinate frame. In this new system, the $\alpha\beta$ axes are fixed at the stator winding

and the $\alpha$-axis is aligned with phase-a axis and the 0-axis is suppressed because the neutral connection of the stator winding is not grounded.

The squirrel-cage induction motor model, expressed in $\alpha\beta 0$ coordinate frame has the following representation:

$$\begin{aligned}\frac{d}{dt}\omega_m &= K_T\boldsymbol{\lambda}_r^\top \mathbf{M}\mathbf{i}_s - \frac{1}{T_m}\omega_m - \frac{1}{J_m}T_L\\ \frac{d}{dt}\boldsymbol{\lambda}_r &= \mathbf{A}_{11}\boldsymbol{\lambda}_r + \mathbf{A}_{12}\mathbf{i}_s\\ \frac{d}{dt}\mathbf{i}_s &= \mathbf{A}_{21}\boldsymbol{\lambda}_r + \mathbf{A}_{22}\mathbf{i}_s + \mathbf{B}_2\mathbf{v}_s\end{aligned} \tag{1}$$

where the rotor flux linkage vector, stator current vector and stator voltage vector, respectively are: $\boldsymbol{\lambda}_r = \begin{bmatrix}\lambda_{\alpha r} & \lambda_{\beta r}\end{bmatrix}^\top$, $\mathbf{i}_s = \begin{bmatrix}i_{\alpha s} & i_{\beta s}\end{bmatrix}^\top$, and $\mathbf{v}_s = \begin{bmatrix}v_{\alpha s} & v_{\beta s}\end{bmatrix}^\top$. The parameter matrices are defined as follows:

$$\mathbf{A}_{11} = \begin{bmatrix}-\frac{1}{T_r} & -\frac{P}{2}\omega_m\\ \frac{P}{2}\omega_m & -\frac{1}{T_r}\end{bmatrix},\quad \mathbf{A}_{12} = \begin{bmatrix}\frac{L_m}{T_r} & 0\\ 0 & \frac{L_m}{T_r}\end{bmatrix},$$

$$\mathbf{A}_{21} = \begin{bmatrix}\frac{\delta}{T_r} & \frac{P}{2}\delta\omega_m\\ -\frac{P}{2}\delta\omega_m & \frac{\delta}{T_r}\end{bmatrix},\quad \mathbf{A}_{22} = \begin{bmatrix}-\gamma & 0\\ 0 & -\gamma\end{bmatrix},$$

$$\mathbf{B}_2 = \begin{bmatrix}\frac{1}{\sigma L_s} & 0\\ 0 & \frac{1}{\sigma L_s}\end{bmatrix},\quad \text{and}\quad \mathbf{M} = \begin{bmatrix}0 & 1\\ -1 & 0\end{bmatrix}.$$

The parameter constants are defined as follows:

$$\sigma = 1 - \frac{L_m^2}{L_s L_r},\quad \delta = \frac{1-\sigma}{\sigma L_m},\ \gamma = \frac{1}{\sigma T_s} + \frac{1-\sigma}{\sigma T_r},\ \text{and}\ K_T = \frac{3P}{4}\frac{L_m}{J_m L_r}.$$

The model parameters are:

$$\begin{aligned}T_s &= \frac{L_s}{R_s},\quad T_r = \frac{L_r}{R_r},\ T_m = \frac{J_m}{B_m},\ L_m = \frac{3}{2}L_{mag},\\ L_r &= L_{ls} + L_m,\quad \text{and } L_r = L'_{lr} + L_m,\end{aligned}$$

where $\omega_m$ is the angular mechanical velocity; $\lambda_{\alpha r}$ and $\lambda_{\beta r}$ are the rotor flux linkages at $\alpha$ and $\beta$ axis, respectively; $i_{\alpha s}$ and $i_{\beta s}$ are the stator currents. $R_s$ is the stator resistance, $R'_r$ is the rotor resistance referred to stator side, $L_{mag}$ is the magnetizing inductance, $L_{ls}$ is the stator leakage inductance, $L'_{lr}$ is the rotor leakage inductance referred to stator winding; all these electric parameter are defined per phase. $P$ is the number of poles; $B_m$ is the shaft frictional coefficient, and $J_m$ is the inertial moment. $T_L$ is load torque and it represents a mechanical input for system (1); $v_{\alpha s}$ and $v_{\beta s}$ are the control inputs. The squirrel-cage induction motor model at $\alpha\beta$ coordinate corresponds to an equivalent two-phase induction motor model, and it is a fifth order non-linear model with constant coefficients.

## III. BLOCK CONTROL LINEARIZATION

The block control method as a linearization technique is applied to non-linear systems to decompose the control synthesis problem into a number of sub-problems of first order which can be solved independently of one another. This is achieved by multiple decomposition of the original system under some structural conditions of unmatched uncertainties. With this technique, a sliding surface is designed to enforce motion according to the specified closed-loop performance [18].

Consider the following general representation of non-linear system subject to uncertainty:

$$\mathbf{x} = \mathbf{f}(\mathbf{x}, t) + \mathbf{B}(\mathbf{x}, t)\,\mathbf{u} + \boldsymbol{\varphi}(\mathbf{x}, t), \tag{2}$$

where $\mathbf{x} \in \mathbf{X} \subset \Re^n$ is the state vector, $\mathbf{u} \in \mathbf{U} \subset \Re^m$ is the control input vector. The columns of matrix $\mathbf{B}$ are smooth and its rank $\mathbf{B}(\mathbf{x}, t) = m$. The unknown mapping $\boldsymbol{\varphi}(\mathbf{x}, t)$ characterizes the external disturbances and parameter variations, which should not affect the feedback system. On the other hand, the essential feature of the block control linearization algorithm is the transformation of the system to the block control form consisting of $r$ blocks as follows [18]:

$$\begin{aligned}\dot{\mathbf{z}}_1 &= -\mathbf{k}_1\mathbf{z}_1 + \mathbf{E}_{11}\mathbf{z}_2 + \boldsymbol{\varphi}_1(\mathbf{z}_1, t)\\ \dot{\mathbf{z}}_i &= -\mathbf{k}_i\mathbf{z}_i + \mathbf{E}_{i1}\mathbf{z}_{i+1} + \boldsymbol{\varphi}_i(\mathbf{z}_i, t),\ i = 2, ..., r-1\\ \dot{\mathbf{z}}_r &= \bar{\mathbf{f}}_r(\mathbf{z}, t) + \bar{\mathbf{B}}_r(\mathbf{z}, t)\,\mathbf{u} + \bar{\boldsymbol{\varphi}}_r(\mathbf{z}, t)\end{aligned} \tag{3}$$

where $\mathbf{z} = [z_1, ..., z_r]^\top$, $\bar{\mathbf{f}}_r(\mathbf{z}, t)$ is a bounded function, and $rank\left(\bar{\mathbf{B}}_r\right) = m$. The process to represent the system (2) in block control form (3) is described in [18] through a recursive transformation. In order to generate sliding mode in (3), a natural choice of the sliding surface is $\mathbf{s} = \mathbf{z}_r$. Then, a specified control law of first order must guarantee the convergence of the closed-loop system motion to manifold $\mathbf{s} = 0$ in a finite time.

Now, in order to transform the induction motor model (1) to the block control form (3), the error variable vector $\mathbf{z}_1$ is defined as follows:

$$\mathbf{z}_1 = \begin{bmatrix}\omega_{ref} - \omega_m\\ \varphi_{ref} - \varphi_r\end{bmatrix} \tag{4}$$

where the output variables to be controlled are: the angular mechanical velocity $\omega_m$ and square modulus of rotor flux linkages $\varphi_r$ which is defined as:

$$\varphi_r = |\,\boldsymbol{\lambda}_r\,|^2 = \boldsymbol{\lambda}_r^\top\boldsymbol{\lambda}_r = \lambda_{\alpha r}^2 + \lambda_{\beta r}^2, \tag{5}$$

meanwhile, $\omega_{ref}$ and $\varphi_{ref}$ are the reference functions for the corresponding output variables. The reference rotor flux considering motor load conditions can be obtained by means of a steady-state analysis of the rotor flux square modulus dynamics, which is calculated by:

$$\frac{d}{dt}\varphi_r = \boldsymbol{\lambda}_r^\top\frac{d}{dt}\boldsymbol{\lambda}_r + \left(\frac{d}{dt}\boldsymbol{\lambda}_r^\top\right)\boldsymbol{\lambda}_r. \tag{6}$$

Using the rotor flux state equation of induction motor model (1) in (6), the squared modulus dynamics of rotor flux linkages can be rewritten as:

$$\frac{d}{dt}\varphi_r = -\frac{2}{T_r}\varphi_r + \frac{2L_m}{T_r}\boldsymbol{\lambda}_r^\top\mathbf{i}_s\,. \tag{7}$$

Considering that, in steady-state, the time variation of rotor flux square modulus is zero, the reference rotor flux $\varphi_{ref}$

is defined solving for the rotor flux square modulus in (7), resulting in:

$$\varphi_{ref} = L_m \boldsymbol{\lambda}_r^\top \mathbf{i}_s. \tag{8}$$

Next, the dynamics of tracking error variables vector (4), that involves the induction motor model (1) and introduces a specified steady first order dynamics, takes the following form:

$$\dot{\mathbf{z}}_1 = \begin{bmatrix} \dot{\omega}_{ref} + \frac{1}{T_m}\omega_m \\ \dot{\varphi}_{ref} + \frac{2}{T_r}\varphi_r \end{bmatrix} - \begin{bmatrix} K_T \boldsymbol{\lambda}_r^\top \mathbf{M} \\ 2\frac{L_m}{T_r}\boldsymbol{\lambda}_r^\top \end{bmatrix} \mathbf{i}_s + \begin{bmatrix} \frac{1}{J_m} T_L \\ 0 \end{bmatrix} = -\mathbf{K}_1 \mathbf{z}_1 \tag{9}$$

where the specified pole matrix $\mathbf{K}_1$, in order to vanish the tracking error variables vector, is:

$$\mathbf{K} = \begin{bmatrix} K_{11} & 0 \\ 0 & K_{22} \end{bmatrix}.$$

With the block control linearization technique, the original system (1) is decomposed into two sub-systems of first order, which can be solved independenly of one another. Then, it is possible to do a control law through stator currents $i_{\alpha s}$ and $i_{\beta s}$, where the reference current vector is defined from (9) by solving for the stator current vector $\mathbf{i}_s$, resulting in:

$$\mathbf{i}_{ref} = \begin{bmatrix} K_T \boldsymbol{\lambda}_r^\top \mathbf{M} \\ 2\frac{L_m}{T_r}\boldsymbol{\lambda}_r^\top \end{bmatrix}^{-1} \left\{ \begin{bmatrix} \dot{\omega}_{ref} + \frac{B_m}{J_m}\omega_m \\ \dot{\varphi}_{ref} + \frac{2}{T_r}\varphi_r \end{bmatrix} + \begin{bmatrix} \frac{1}{J_m} T_L \\ 0 \end{bmatrix} + \mathbf{K}_1 \mathbf{z}_1 \right\} \tag{10}$$

Afterwards, a second error variable vector is defined by currents as follows:

$$\mathbf{z}_2 = \mathbf{i}_{ref} - \mathbf{i}_s, \tag{11}$$

and its dynamics is:

$$\dot{\mathbf{z}}_2 = \mathbf{F}\left(\boldsymbol{\lambda}_r, \mathbf{z}_1, \mathbf{z}_2\right) - \mathbf{B}_2 \mathbf{v}_s, \tag{12}$$

where:

$$\mathbf{f}\left(\boldsymbol{\lambda}_r, \mathbf{z}_1, \mathbf{z}_2\right) = \frac{d}{dt}\mathbf{i}_{ref} - \begin{bmatrix} \frac{\delta}{T_r} & \frac{P}{2}\delta\left(\omega_{ref} - \varepsilon_w\right) \\ -\frac{P}{2}\delta\left(\omega_{ref} - \varepsilon_w\right) & \frac{\delta}{T_r} \end{bmatrix} \boldsymbol{\lambda}_r + \gamma\left(\mathbf{i}_{ref} - \mathbf{z}_2\right),$$

and

$$\mathbf{B}_2 = \begin{bmatrix} \frac{1}{\sigma L_s} & 0 \\ 0 & \frac{1}{\sigma L_s} \end{bmatrix}.$$

Finally, using (9), (12) and one steady state equation from system (1) as zero dynamics, the equivalent representation of induction motor model (1) in the block control form (3) is obtained as follows:

$$\begin{aligned} \dot{\mathbf{z}}_1 &= -\mathbf{K}_1 \mathbf{z}_1 + \begin{bmatrix} K_T \boldsymbol{\lambda}_r^\top \mathbf{M} \\ 2\frac{L_m}{T_r}\boldsymbol{\lambda}_r^\top \end{bmatrix} \mathbf{z}_2 \\ \dot{\mathbf{z}}_2 &= \mathbf{F}\left(\boldsymbol{\lambda}_r, \mathbf{z}_1, \mathbf{z}_2\right) - \mathbf{B}_2 \mathbf{v}_s \end{aligned}$$

$$\dot{\lambda}_{\alpha r} = -\frac{1}{T_r}\lambda_{\alpha r} - \frac{P}{2}\left(\omega_{ref} - \varepsilon_\omega\right)\lambda_{\beta r} + \frac{L_m}{T_r} i_{\alpha s} \tag{13}$$

The state equation of rotor flux linkage $\lambda_{\alpha r}$ in (13) represents an internal dynamics to complete the order of the original system (1). It is important to remark that the main advantage of the block control linearization technique is its symplicity where the control input vector is decoupled and the system (13) is ready to apply a specified first order control law, which steers the tracking current error vector $\mathbf{z}_2$ towards zero, and afterward, $\mathbf{z}_2$ steers the tracking error vector $\mathbf{z}_1$ asymptotically to the origin. This control law can be the super-twisting algorithm due to its robustness shown in different applications for non-linear systems [13], [21]–[23].

## IV. SUPER-TWISTING CONTROLLER

The sliding mode is an efficient tool for controlling high order complex systems that works under uncertain conditions. The first order sliding modes are induced in closed-loop systems by a discontinuous control input whose argument is a mathematical function known as sliding surface, which is designed through the block control approach proposed. The discontinuous input switches to high frequency and it ensures the state variables movement toward the sliding surface [3]. The movement through the sliding surface is named sliding modes. The high switching frequency produces an effect known as chattering effect, which may manifest as very high frequency vibrations in a controlled system [3].

On the order hand, high order sliding modes use the basic concept of the conventional sliding modes for the high order derivatives of the system to be controlled. Therefore, the second order sliding modes are characterized by having a continuous control signal bounded dependent at time, with discontinuities only in the control's derivative [3]. This feature helps to reduce significantly the chattering effect. The super-twisting controller, being a second-order algorithm, is applied to systems where control appears in the first derivative of the sliding variable. Some characteristics of the super-twisting controller are: it compensates uncertainties that are Lipschitz, it uses only the sliding surface as argument, it provides finite-time convergence to the origin for the sliding surface and its time derivative, and it generates a continuous control signal.

The sliding surface is defined from the system representation in block control form (13), for the variable where the control input appears in its state equation, *i.e.* the block $r$ in system (3), then:

$$\mathbf{s} = \mathbf{z}_2, \tag{14}$$

To induce sliding mode in $\mathbf{s} = 0$ (14), (11) and in its time derivative $\dot{\mathbf{s}} = 0$ (12), the super-twisting algorithm is applied with the following vector representation:

$$\mathbf{v}_s = \boldsymbol{\lambda}|\mathbf{s}|^{\frac{1}{2}} \operatorname{sign} \mathbf{s} + \mathbf{v}_{s1}, \tag{15}$$

where $\dot{\mathbf{v}}_{s1} = \boldsymbol{\alpha} \operatorname{sign} \mathbf{s}$, $\boldsymbol{\lambda} = \begin{bmatrix} \lambda_\alpha & 0 \\ 0 & \lambda_\beta \end{bmatrix}$, and $\boldsymbol{\alpha} = \begin{bmatrix} \alpha_\alpha & 0 \\ 0 & \alpha_\beta \end{bmatrix}$.

The diagonal matrix $\lambda$ and $\alpha$ have components that can be selected according to the sufficient conditions described by [19], in such a way that the sliding surface (14) converges to zero in finite time. Once the control law (15) is substituted in the block control form (13), it results in:

$$\begin{aligned}\dot{\mathbf{z}}_1 &= -\mathbf{K}_1\mathbf{z}_1 + \begin{bmatrix} K_T\boldsymbol{\lambda}_r^\top\mathbf{M} \\ 2\frac{L_m}{T_r}\boldsymbol{\lambda}_r^\top \end{bmatrix}\mathbf{z}_2 \\ \dot{\mathbf{z}}_2 &= \mathbf{F}\left(\boldsymbol{\lambda}_r, \mathbf{z}_1, \mathbf{z}_2\right) - \mathbf{B}_2\left(\boldsymbol{\lambda}|\mathbf{s}|^{\frac{1}{2}}\operatorname{sign}\mathbf{s} + \mathbf{v}_{s1}\right) \\ \dot{\mathbf{v}}_{s1} &= \boldsymbol{\alpha}\ \operatorname{sign}\mathbf{s} \\ \dot{\lambda}_{\alpha r} &= -\frac{1}{T_r}\lambda_{\alpha r} - \frac{P}{2}\left(\omega_{ref} - \varepsilon_\omega\right)\lambda_{\beta r} + \frac{L_m}{T_r}i_{\alpha s}. \end{aligned} \quad (16)$$

Selecting the sliding surface as (14), a new reduced order system results in:

$$\begin{aligned}\dot{\mathbf{s}} &= \mathbf{F}\left(\boldsymbol{\lambda}_r, \mathbf{z}_1, \mathbf{s}\right) - \mathbf{B}_2\left(\boldsymbol{\lambda}|\mathbf{s}|^{\frac{1}{2}}\operatorname{sign}\mathbf{s} + \mathbf{v}_{s1}\right) \\ \dot{\mathbf{v}}_{s1} &= \boldsymbol{\alpha}\ \operatorname{sign}\mathbf{s}. \end{aligned} \quad (17)$$

In order to simplify the stability analysis, the system (17) can be handled in its scalar form as follows:

$$\begin{aligned}\dot{s}_i &= -k_{1i}\,|s_i|^{\frac{1}{2}}\operatorname{sign}(s_i) + u_i + f_i \\ \dot{u}_i &= -k_{2i}\operatorname{sign}(s_i), \quad i = \alpha, \beta. \end{aligned} \quad (18)$$

where:

$$\begin{aligned}\begin{bmatrix} k_{1\alpha} & k_{1\beta} \end{bmatrix}^\top &= \mathbf{B}_2\boldsymbol{\lambda}, \\ \begin{bmatrix} k_{2\alpha} & k_{2\beta} \end{bmatrix}^\top &= \mathbf{B}_2\boldsymbol{\alpha}, \\ \begin{bmatrix} u_\alpha & u_\beta \end{bmatrix}^\top &= \mathbf{B}_2\mathbf{v}_{s1}. \end{aligned} \quad (19)$$

Based on [19], the stability analysis is obtained from the closed-loop system using the super-twisting algorithm as control law. Then the following transformation is proposed:

$$\zeta_i = \begin{bmatrix} |s_i|^{\frac{1}{2}}\operatorname{sign}(s_i) & u_i \end{bmatrix}^\top, \quad |\zeta_{1i}| = |s_i|^{\frac{1}{2}},\ i = d, q. \quad (20)$$

with its time derivative as:

$$\dot{\zeta}_i = \frac{1}{|\zeta_{1i}|}\begin{bmatrix} \frac{1}{2}\left(-k_{1i}\zeta_{1i} + \zeta_{2i} + f_i\right) & -k_{2i}\zeta_{1i} \end{bmatrix}^\top. \quad (21)$$

Where the equation (21) is expressed as the following linear system:

$$\dot{\boldsymbol{\zeta}}_i = \mathbf{A}_i\boldsymbol{\zeta}_i + \boldsymbol{\rho}_i \quad (22)$$

with $\mathbf{A}_i = \frac{1}{|\zeta_{1i}|}\begin{bmatrix} -\frac{1}{2}k_{1i} & \frac{1}{2} \\ -k_{2i} & 0 \end{bmatrix}$, $\boldsymbol{\rho}_i = \begin{bmatrix} \frac{1}{2|\zeta_{1i}|}f_i \\ 0 \end{bmatrix}$,

$|\zeta_{1i}| = |s_i|^{\frac{1}{2}}$, and $f_i$ is bounded with the following restrictions:

$$|f_i| \le \delta_i|s_i|^{\frac{1}{2}}, \quad |f_i| \le \delta_i|\zeta_{1i}|, \quad \delta_i \ge 0. \quad (23)$$

In order to analyze the stability condition of the new system (22), a Lyapunov function candidate is proposed as follows [19]:

$$V_i(\boldsymbol{\zeta}) = \boldsymbol{\zeta}_i^\top\mathbf{P}_i\boldsymbol{\zeta}_i, \quad (24)$$

where

$$\mathbf{P}_i = \frac{1}{2}\begin{bmatrix} 4k_{2i} + k_{1i}^2 & -k_{1i} \\ -k_{1i} & 2 \end{bmatrix}.$$

Deriving the Lyapunov function along the trajectories of the system, the Lyapunov function dynamic equation is obtained as:

$$\dot{V}_i\left(\boldsymbol{\zeta}_i\right) = \boldsymbol{\zeta}_i^\top\left(\mathbf{A}_i^\top\mathbf{P}_i + \mathbf{P}_i\mathbf{A}_i\right)\boldsymbol{\zeta}_i + 2\boldsymbol{\zeta}_i^\top\mathbf{P}_i\boldsymbol{\rho}_i. \quad (25)$$

Assuming that $f_i$ in (18) is an external disturbance bounded by:

$$f_i = \delta_i|s_i|^{\frac{1}{2}}\operatorname{sign}(s_i) = \delta_i\zeta_{1i}. \quad (26)$$

Involving (26) in the term $\boldsymbol{\rho}$ of (25) yields:

$$\dot{V}_i\left(\boldsymbol{\zeta}_i\right) = -\frac{1}{|\zeta_{1i}|}\boldsymbol{\zeta}_i^\top\mathbf{Q}_i\boldsymbol{\zeta}_i, \quad (27)$$

where

$$\mathbf{Q}_i = \frac{k_{1i}}{2}\begin{bmatrix} k_{1i}^2 + 2k_{2i} - \delta_i\left(k_{1i} + 4\frac{k_{2i}}{k_{1i}}\right) & -k_{1i} \\ -\left(k_{1i} - \delta_i\right) & 1 \end{bmatrix}.$$

The matrix $\mathbf{Q}_i$ must be positive definite, then $k_{1i}$ and $k_{2i}$ values should fulfill the following conditions:

$$\begin{aligned} k_{1i} &> 2\delta_i \\ k_{2i} &> \frac{1}{2}\frac{k_{1i}^2\left(\delta_i - k_{1i}\right)}{k_{1i} - 2\delta_i} \end{aligned} \quad (28)$$

Consequently, the controller gains $\lambda_i$ and $\alpha_i$ in (19) are selected such that the following conditions are satisfied:

$$\begin{aligned} \lambda_i &> 2\sigma L_s\delta_i \\ \alpha_i &> \frac{1}{2}\frac{\sigma L_s k_{1i}^2\left(\delta_i - k_{1i}\right)}{k_{1i} - 2\delta_i} \end{aligned} \quad (29)$$

Hence, the time derivative of system (27) is negative definite and asymptotic stability is ensured. Then, the control restrictions (29) for $\lambda_i$ and $\alpha_i$ provide finite time attractively of the sliding mode on the set $s = 0$ and $\dot{s} = 0$ and an asymptotic movement of the tracking error variable $\mathbf{z}_1$ is presented.

## V. ROTOR FLUX AND LOAD TORQUE OBSERVERS

An asymptotic state observer is a dynamic system that provides an estimate of the internal state of a physics system using measurements of its input and output directly [1]. In this work, a robust observer is designed to estimate the rotor flux linkages, and after that, an asymptotic load torque observer is introduced.

### A. ROTOR FLUX LINKAGES OBSERVER DESIGN

Let us consider the linear time-invariant systems:

$$\dot{x} = Ax + Bu, \quad (30)$$

with the measured output variables given by:

$$y = Cx, \quad (31)$$

where $y \in \Re^m$, $C$ is a constant and $\operatorname{rank}(C) = m$. It is possible to represent the system output as $y = C_1x_1 + C_2x_2$,

to separate the unmeasurable $x_1$ and measurable variables $x_2$. Then writing the equation of system (30) and its output (31) at space $[x_1 \;\; y]^\top$ through the following transformation matrix:

$$T = \begin{bmatrix} I_{n-m} & 0 \\ C_1 & C_2 \end{bmatrix} \tag{32}$$

results:

$$\begin{aligned} \dot{x}_1 &= A_{11}x_1 + A_{12}y + B_1 u \\ y &= A_{21}x_1 + A_{22}y + B_2 u \end{aligned} \tag{33}$$

where

$$TAT^{-1} = \begin{bmatrix} A_{11} & A_{12} \\ A_{21} & A_{22} \end{bmatrix}, \quad TB = \begin{bmatrix} B_1 \\ B_2 \end{bmatrix}.$$

Now, in order to achieve robustness in the state-observer design, inputs are added as discontinuous functions of mismatches at system, yielding the following observer design [1]:

$$\begin{aligned} \dot{\hat{x}}_1 &= A_{11}\hat{x}_1 + A_{12}\hat{y} + B_1 u - G_1 v \\ \dot{\hat{y}} &= A_{21}\hat{x}_1 + A_{22}\hat{y} + B_2 u + v \end{aligned} \tag{34}$$

where $\hat{x}_1$ and $\hat{y}$ are the estimates of the system state, $v = N \operatorname{sign}(y - \hat{y})$, $N > 0$ and it is selected to force that the surface $s = y - \hat{y} = 0$ to be reached. The matrix $G_1$ must be determined such that the observation error $\tilde{x}_1 = x_1 - \hat{x}_1$ decays at the specified rate.

Then, the robust observer design process (34) applied to estimate the rotor flux linkages of the squirrel-cage induction motor results in a dynamic model defined as:

$$\begin{aligned} \frac{d}{dt}\hat{\boldsymbol{\lambda}}_r &= \mathbf{A}_{11}\hat{\boldsymbol{\lambda}}_r + \mathbf{A}_{12}\hat{\mathbf{i}}_s - \mathbf{G}_1\mathbf{v} \\ \frac{d}{dt}\hat{\mathbf{i}}_s &= \mathbf{A}_{21}\hat{\boldsymbol{\lambda}}_r + \mathbf{A}_{22}\hat{\mathbf{i}}_s + \mathbf{B}_2\mathbf{v}_s + \mathbf{v} \end{aligned} \tag{35}$$

where $\mathbf{v} = \mathbf{N} \operatorname{sign}\left(\mathbf{i}_s - \hat{\mathbf{i}}_s\right)$, $\mathbf{N} = \begin{bmatrix} N_{11} & 0 \\ 0 & N_{22} \end{bmatrix}$, and $\mathbf{G}_1 = \begin{bmatrix} G_{11} & 0 \\ 0 & G_{22} \end{bmatrix}$, and with $\hat{\boldsymbol{\lambda}}_r$ that represents the observed rotor flux vector and $\hat{\mathbf{i}}_s$ is the observed stator current vector. The discontinuous function $\mathbf{v}$ is chosen such that sliding mode is enforced in the surface $\mathbf{s} = \mathbf{i}_s - \hat{\mathbf{i}}_s = 0$ defined by the stator currents observation error, and $\mathbf{N}$ is a diagonal matrix, where the components have high enough positive values for steering the surface toward zero in finite time. Meanwhile matrix $G_1$ must satisfy vanishing of the rotor fluxes observation error vector $\boldsymbol{\lambda}_s = \boldsymbol{\lambda}_s - \hat{\boldsymbol{\lambda}}_s = 0$ on the specified rate [1].

In order to guarantee the convergence of the proposed state observer, it is necessary to do an analysis of the observation error dynamics. From induction motor model (1) and the rotor fluxes observer (35), the observation error dynamics is defined and it takes the following form:

$$\begin{aligned} \frac{d}{dt}\tilde{\boldsymbol{\lambda}}_r &= \mathbf{A}_{11}\tilde{\boldsymbol{\lambda}}_r + \mathbf{A}_{12}\tilde{\mathbf{i}}_s + \mathbf{G}_1\mathbf{v} \\ \frac{d}{dt}\tilde{\mathbf{i}}_s &= \mathbf{A}_{21}\tilde{\boldsymbol{\lambda}}_r + \mathbf{A}_{22}\tilde{\mathbf{i}}_s - \mathbf{v} \end{aligned} \tag{36}$$

When the sliding mode is forced into the surface $\tilde{\mathbf{i}}_s = \mathbf{i}_s - \hat{\mathbf{i}}_s = 0$, the input $\mathbf{v}$ becomes the equivalent control $v_{eq}$ of system (36). By solving equation $\frac{d}{dt}\tilde{\mathbf{i}}_s = 0$, the equivalent control $v_{eq}$ takes the form:

$$v_{eq} = A_{21}\tilde{\boldsymbol{\lambda}}_r. \tag{37}$$

Substituting (37) into system (36), yields the following homogeneous equation:

$$\frac{d}{dt}\tilde{\boldsymbol{\lambda}}_r = \left(\mathbf{A}_{11} + \mathbf{G}_1\mathbf{A}_{21}\right)\tilde{\boldsymbol{\lambda}}_r. \tag{38}$$

Hence, the specified rate of convergence of $\tilde{\boldsymbol{\lambda}}_r$ to zero, *i.e.* convergence of $\hat{\boldsymbol{\lambda}}_r$ to $\boldsymbol{\lambda}_r$, is provided by a proper selection of matrix $\mathbf{G}_1$. The observer with the input as discontinuous function of the error $\tilde{\mathbf{i}}_s = \mathbf{i}_s - \hat{\mathbf{i}}_s$ ensures its convergence even in presence of unmodeled disturbances. In addition, the observer presents robustness in presence of noise; therefore, this nonlinear observer has great filtering properties [1].

### B. LOAD TORQUE OBSERVER DESIGN

The mechanical model of the induction motor, including the load torque equation with smooth movement, has the following representation:

$$\begin{aligned} \frac{d}{dt}\omega_m &= K_T\boldsymbol{\lambda}_r^\top\mathbf{M}\mathbf{i}_s - \frac{1}{T_m}\omega_m - \frac{1}{J_m}T_L \\ \frac{d}{dt}T_L &\approx 0. \end{aligned} \tag{39}$$

On the other hand, the asymptotic load torque observer for the squirrel-cage induction motor has the following form:

$$\begin{aligned} \frac{d}{dt}\hat{\omega}_m &= K_T\boldsymbol{\lambda}_r^\top\mathbf{M}\mathbf{i}_s - \frac{1}{T_m}\hat{\omega}_m - \frac{1}{J_m}\hat{T}_L + l_1\left(\omega_m - \hat{\omega}_m\right) \\ \frac{d}{dt}\hat{T}_L &= l_2\left(\omega_m - \hat{\omega}_m\right) \end{aligned} \tag{40}$$

where $\hat{\omega}_m$ is the observed angular mechanical velocity, $\hat{T}_L$ is the observed load torque, $l_1$ and $l_2$ are constants, which are selected to ensure the asymptotic convergence to zero at specified rate of the angular velocity observation error $\tilde{\omega}_m = \omega_m - \hat{\omega}_m$.

In order to guarantee the convergence of the proposed load torque observer, it is necessary to do an analysis of the observation error dynamics. From the mechanical model (39) and the load torque observer (40), the observation error dynamics is:

$$\begin{bmatrix} \frac{d}{dt}\tilde{\omega}_m \\ \frac{d}{dt}\tilde{T}_L \end{bmatrix} = \begin{bmatrix} -\left(\frac{1}{T_m} + l_1\right) & -\frac{1}{J_m} \\ -l_2 & 0 \end{bmatrix} \begin{bmatrix} \tilde{\omega}_m \\ \tilde{T}_L \end{bmatrix}. \tag{41}$$

In order to relocate the poles of system (41) at the stable region by means $l_1$ and $l_2$, the characteristic polynomial is defined as:

$$\lambda^2 + \left(\frac{1}{T_m} + l_1\right)\lambda - \frac{l_2}{J_m} = 0, \tag{42}$$

**FIGURE 2.** Work-bench to design control systems for electrical machines.

where the constants $l_1$ and $l_2$ are calculated by the specified poles $p_1$ and $p_2$, such that the observation error movement decreases to zero. Then, $l_1$ and $l_2$ are defined as follows:

$$\begin{aligned} l_1 &= p_1 + p_2 - \frac{1}{T_m} \\ l_2 &= -p_1 p_2 J_m \end{aligned} \tag{43}$$

and $\hat{\omega}_m$ converges to $\omega_m$ in finite time, and consequently, the load torque is estimated by (40).

## VI. EXPERIMENTAL RESULTS

The experimental validation of the proposed velocity controller for the squirrel-cage induction motor was carried out under a velocity tracking test in a work-bench that contains the following equipment:

1) A squirrel-cage induction motor coupled to a wound-rotor induction machine which has assembled a BEI incremental encoder mounted on its shaft. This encoder measures the angular mechanical velocity with a resolution of 2048 pulses per revolution.
2) A dSpace DS1103 data acquisition board with RTI interface for signal visualization.
3) A SEMIKRON three-phase inverter, bridge type.
4) A measuring interface consisting of three current sensors, one each per phase.
5) A signal conditioning interface for coupling the SVPWM signal from DS1103 board to the activation circuit of the IGBT's gates.

A work-bench picture is shown in Fig. 2, and the rated values and parameters of the motor are reported in Table 1. In order to validate the robustness of the closed-loop velocity controller using block control linearization technique combined with the super-twisting algorithm a velocity tracking test was carried out with a sampling time of 240 $\mu s$

### A. TRACKING OF CONTROLLED OUTPUTS

The controlled outputs are the angular mechanical velocity $\omega_m$ and the square modulus of the rotor flux linkages $\varphi_r$. A tracking test is configured, where the angular velocity of the induction motor tracks a reference function defined by a periodic square function (pulse train) that varies from 1,820 to 1,900 $r.p.m.$ with a period of 5 $s$. Meanwhile, the rotor flux square modulus tracks a reference function defined by internal product between stator current vector and rotor flux vector, regarding to equation (8). The velocity tracking has an effective performance when the induction motor velocity tracks the reference signal, see Fig. 3 a). The angular mechanical velocity has a rise time of 152 $ms$ with an overshoot of 12.5 % when the reference suddenly increases, and a falling time of 110 $ms$ with an overshoot of 28 % when the reference suddenly decreases. Fig. 3 b) shows that the square modulus signal of rotor flux linkages effectively tracks its reference signal, which varies according to the stator current variations due to changes in the mechanical load. In steady sate, the tracking performance of rotor flux square modulus is acceptable and the reference value is attenuated only by the inductance $L_m$, as defined in equation (8). While in the transient stage, the rotor flux square modulus presents overshoots due to the sudden increase of the stator currents and to the reciprocal value of the rotor time constant $T_r$; this is according to transient equation (7).

**TABLE 1.** Rated values and motor model parameters.

| Parameter | Value |
|---|---|
| Power | 3/4 $HP$ |
| Line to line rated voltage | 208-230/460 $V$ |
| Rated current | 3.2-3/1.5 $A$ |
| Rated angular velocity | 1725 $r.p.m.$ |
| Stator resistance, $R_s$ | 2.5 $\Omega$ |
| Rotor resistance, $R_r$ | 2.7 $\Omega$ |
| Stator inductance, $L_s$ | 0.2260 $H$ |
| Magnetizing inductance, $L_m$ | 0.2165 $H$ |
| Rotor Inductance, $L_r$ | 0.2260 $H$ |
| Inertial moment, $J_m$ | 0.0055 $Nms^2$ |
| Frictional coefficient, $B_m$ | 0.0018 $Nms$ |

### B. VELOCITY CONTROLLER PERFORMANCE

In order to obtain a robust closed-loop system, the block control linearization technique is combined with the super-twisting algorithm. The sliding surface vector is defined by the stator currents tracking on $\alpha$ and $\beta$ axes (11), and this surface is defined with the linearization technique (14) and it represents the argument of the super-twisting control law (15). Fig. 4 a) displays the stator currents tracking on $\alpha$ and $\beta$ axes, these currents oscillate between 3.0 $A$ and -3.0 $A$ when the motor runs at 1,820 $r.p.m.$, and they oscillate between 4.0 $A$ and -4.0 $A$ at 1,900 $r.p.m.$, both values are measured in steady state. In Fig. 4 b), the sliding surfaces on the $\alpha$ and $\beta$ axes (14) are depicted. In steady state, the amplitude of these sliding surfaces are 0.6 $A$ at 1,820 $r.p.m.$ and 0.8 $A$ at 1,900 $r.p.m.$, approximately. The control inputs on on $\alpha$ and $\beta$ axes are shown in Fig. 4 c). These inputs are decoupled with respect to state variables $\mathbf{z}_1$ and $\mathbf{z}_2$ in the block control form (13), where the input vector is $\mathbf{v}_s = \begin{bmatrix} v_\alpha & v_\beta \end{bmatrix}^\top$. Both inputs oscillate between 115 $V$ and

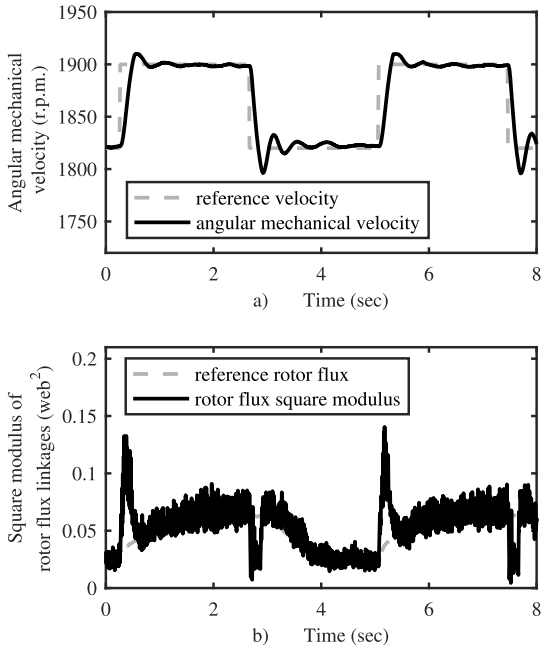


**FIGURE 3.** Tracking performance: a) angular mechanical velocity, and b) rotor flux square modulus.

-115 $V$ at 1,800 $r.p.m.$ and they oscillate between 150 $V$ and -150 $V$ at 1,900 $r.p.m.$, approximately. According to the similitude transformation to refer the variables from frame $abc$ to frame $\alpha\beta 0$, the voltage on the $\alpha$ axis corresponds to the phase $A$ voltage that feeds the stator winding. The super-twisting algorithm, according to (15), was tuned with control gains of $\lambda_\alpha = 170$, $\alpha_\alpha = 180$ for controlling the angular mechanical velocity, and $\lambda_\beta = 135$, $\alpha_\beta = 80$ for controlling the square modulus of the rotor flux linkages. These control gains accomplish the inequalities (29), where the disturbance modulus of the reduced system (18) is defined in (23). The IGBT's three-phase inverter uses the space vector pulse width modulation (SVPWM) technique for conditioning the two control inputs $v_\alpha$ and $v_\beta$ and can be adjusted the three-phase voltage supply for feeding the stator winding. The three-phase inverter worked with switching frequency of 18,720 $Hz$ and with a CD-bus voltage of 265 $V$.

### C. ROTOR FLUX OBSERVER PERFORMANCE

The robust observer of rotor flux linkages includes a discontinuous input vector (first order sliding modes), whose argument is the current observer error vector, to provide robustness in the estimation of rotor flux linkages on $\alpha\beta$ coordinate frame. The gains of these discontinuous inputs are the components of the diagonal matrix $\mathbf{N}$ in equation (35), with values of $N_{11} = 500$, and $N_{22} = 450$ to enforce the current observer error vector to the surface $\mathbf{s} = \mathbf{i}_s - \hat{\mathbf{i}}_s = 0$. Then, in Fig. 5 a), it can be seen that the estimated rotor current on $\alpha$ axis converges to the real stator current. Once the observer error convergence of stator currents is achieved, the rotor flux linkages vector $\boldsymbol{\lambda}_r$ converges toward its estimated value with the gains $G_{11} = 0.015$ and $G_{22} = 0.020$, due to the rotor

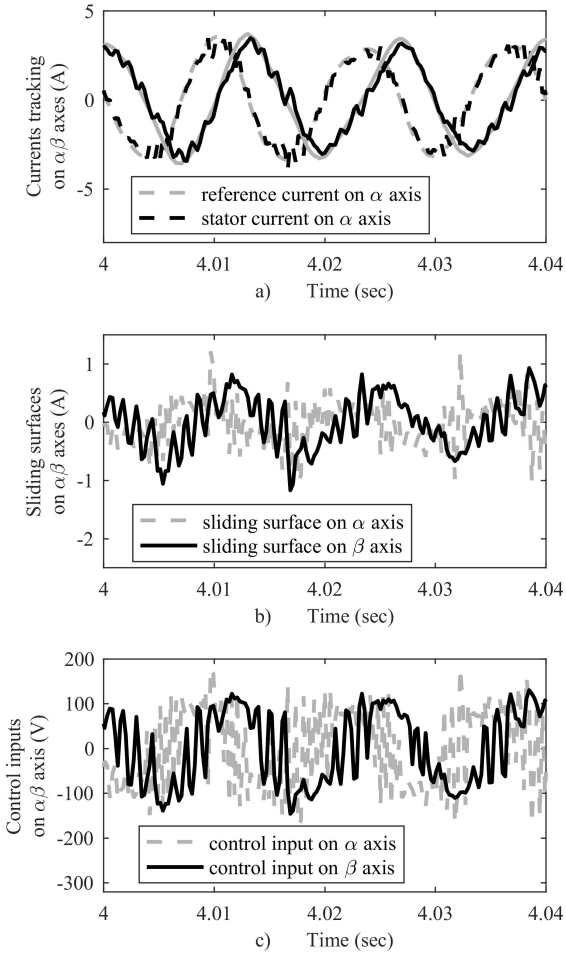


**FIGURE 4.** Performance of the velocity controller.

flux estimation error converge to zero asymptotically in finite time, according to equation (38), see Fig. 5 b). The tuning of the rotor flux linkages observer was carried out in real-time using the proposed work-bench.

### D. LOAD TORQUE OBSERVER PERFORMANCE

The asymptotic observer to estimate the induction motor load torque was designed taking into account the mechanical model of the induction motor (39). The velocity observer error (41) converges to zero using the gains $l_1 = 120$, and $l_2 = -20$, (see Fig. 6 a)), and as consequence, the load torque converges to its estimated value (40), (see Fig. 6 b)). The tuning of the load torque observer was carried out in real-time using the proposed work-bench.

## VII. CONCLUSION

On this paper, a robust non-linear velocity controller applied to the squirrel-cage induction motor under variable load conditions has been proposed and validated with graphic results obtained in real-time. The load is represented by the coupled induction generator which delivers power toward the utility grid above synchronous velocity. The super-twisting algorithm is applied as control law whose argument is a sliding

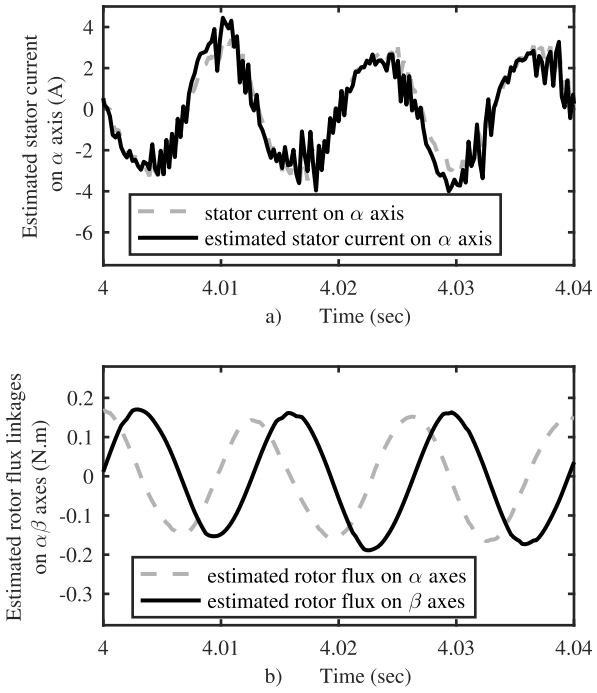


**FIGURE 5.** Performance of the rotor flux observer on $\alpha - \beta$ axes.

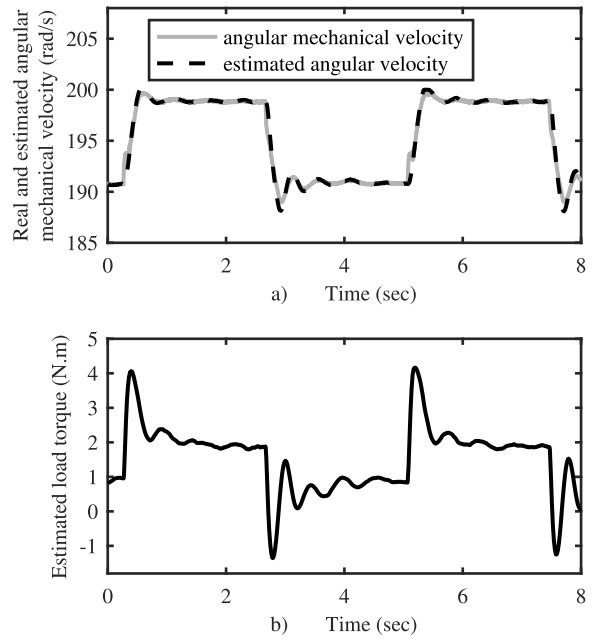


**FIGURE 6.** Performance of the load torque observer.

manifold which is designed by the block control linearization technique. Furthermore, a non-linear sliding mode observer for estimating the rotor flux linkages on $\alpha$ and $\beta$ axes is designed because these variables are not available, and a Luenberger reduced observer is designed for estimating the load torque, which is considered an external disturbance for the system. These estimated variables are necessary for the design of the controller. In order to validate the robustness of the proposed controller, including the observers, work-bench real-time results are presented. A pulse train above synchronous velocity, as a reference signal in the velocity tracking, is configured; where the step function is presented in two cases, when the velocity suddenly rises and when it suddenly falls. Meanwhile, the reference rotor flux varies with the stator current values i.e. load conditions of the induction motor. Therefore, the control goal of the proposed controller is achieved in a satisfactory way by solving the velocity tracking problem applying block control linearization technique through the current control in combination with the super-twisting algorithm as control law and tuning the observers designed, as illustrated by the Figs. 3 - 6.

## REFERENCES

[1] V. Utkin, J. Guldner, and J. Shi, *Sliding Mode Control in Electro-Mechanical Systems*, vol. 34. Boca Raton, FL, USA: CRC Press, 2009.

[2] V. I. Utkin, "Sliding mode control design principles and applications to electric drives," *IEEE Trans. Ind. Electron.*, vol. 40, no. 1, pp. 23–36, Feb. 1993.

[3] L. Fridman and A. Levant, "Higher order sliding modes as a natural phenomenon in control theory," in *Robust Control Via Variable Structure and Lyapunov Techniques*. Berlin, Germany: Springer, 1996, pp. 107-133.

[4] A. Chalanga, S. Kamal, L. M. Fridman, B. Bandyopadhyay, and J. A. Moreno, "Implementation of super-twisting control: Super-twisting and higher order sliding-mode observer-based approaches," *IEEE Trans. Ind. Electron.*, vol. 63, no. 6, pp. 3677–3685, Jun. 2016.

[5] Y. Shtessel, C. Edwards, L. Fridman, and A. Levant, *Sliding Mode Control and Observation*, vol. 10. New York, NY, USA: Birkhäuser, 2014.

[6] P. Krause, O. Wasynczuk, S. D. Sudhoff, and S. Pekarek, *Analysis of Electric Machinery and Drive Systems*, vol. 75. Hoboken, NJ, USA: Wiley, 2013.

[7] C. M. R. Oliveira, M. L. Aguiar, J. R. B. A. Monteiro, W. C. A. Pereira, G. T. Paula, and T. E. P. Almeida, "Vector control of induction motor using an integral sliding mode controller with anti-windup," *J. Control, Autom. Elect. Syst.*, vol. 27, no. 2, pp. 169–178, Apr. 2016.

[8] C. Lascu and F. Blaabjerg, "Super-twisting sliding mode direct torque contol of induction machine drives," in *Proc. IEEE Energy Convers. Congr. Expo. (ECCE)*, Sep. 2014, pp. 5116–5122.

[9] F. Alonge, M. Cirrincione, F. D'Ippolito, M. Pucci, and A. Sferlazza, "Robust active disturbance rejection control of induction motor systems based on additional sliding-mode component," *IEEE Trans. Ind. Electron.*, vol. 64, no. 7, pp. 5608–5621, Jul. 2017.

[10] H. Tohidi, K. Erenturk, and S. Shoja-Majidabad, "Passive fault tolerant control of induction motors using nonlinear block control," *Control Eng. Appl. Inform.*, vol. 19, no. 1, pp. 49–58, 2017.

[11] H. Sira-Ramírez, F. González-Montañez, J. A. Cortés-Romero, and A. Luviano-Juárez, "A robust linear field-oriented voltage control for the induction motor: Experimental results," *IEEE Trans. Ind. Electron.*, vol. 60, no. 8, pp. 3025–3033, Aug. 2013.

[12] D. Honório, E. Diniz, A. B. de Souza, O. M. Almeida, and L. Barreto, "Comparison between sliding model control and vector control for a DSP-based position control applied to squirrel-cage induction motor," in *Proc. 9th IEEE/IAS Int. Conf. Ind. Appl. (INDUSCON)*, Nov. 2010, pp. 1–6.

[13] F. A. Valenzuela, O. A. Morfin, R. J. Rodríguez, J. Ramírez, and M. I. Castellanos, "High performance controller design applied to the induction motor via quasi-continuous SOSM," in *Proc. 22nd Int. Conf. Elect. Commun. Comput. (CONIELECOMP)*, Feb. 2012, pp. 124–129.

[14] J. R. Dominguez, C. Mora-Soto, S. Ortega-Cisneros, J. J. R. Panduro, and A. G. Loukianov, "Copper and core loss minimization for induction motors using high-order sliding-mode control," *IEEE Trans. Ind. Electron.*, vol. 59, no. 7, pp. 2877–2889, Jul. 2012.

[15] P. C. Sen, *Principles of Electric Machines and Power Electronics*. Hoboken, NJ, USA: Wiley, 2007.

[16] D. Bullo, A. Ferrara, and M. Rubagotti, "Sliding mode observers for sensorless control of current-fed induction motors," in *Proc. Amer. Control Conf. (ACC)*, Jun./Jul. 2011, pp. 763–768.

[17] A. Derdiyok, Z. Yan, M. Guven, and V. Utkin, "A sliding mode speed and rotor time constant observer for induction machines," in *Proc. 27th Annu. Conf. Ind. Electron. Soc. (IECON)*, vol. 2. Nov./Dec. 2001, pp. 1400–1405.
[18] A. G. Loukianov, "Robust block decomposition sliding mode control design," *Math. Problems Eng.*, vol. 8, nos. 4–5, pp. 349–365, 2002.
[19] A. Dávila, J. A. Moreno, and L. Fridman, "Optimal Lyapunov function selection for reaching time estimation of super twisting algorithm," in *Proc. 48th IEEE Conf. Decision Control, Held Jointly 28th Chin. Control Conf. (CDC/CCC)*, Dec. 2009, pp. 8405–8410.
[20] A. A. Z. Diab and V. V. Pankratov, "Sliding mode control of vector controlled induction motor drive," in *Proc. 11th Int. Conf. Actual Problems Electron. Instrum. Eng. (APEIE)*, Oct. 2012, pp. 114–121.
[21] O. A. Morfin, C. E. Castañeda, A. Valderrabano-Gonzalez, M. Hernandez-Gonzalez, and F. A. Valenzuela, "A real-time SOSM super-twisting technique for a compound DC motor velocity controller," *Energies*, vol. 10, no. 9, p. 1286, 2017.
[22] O. A. Morfin, R. Ruiz-Cruz, A. G. Loukianov, E. N. Sánchez, M. I. Castellanos, and F. A. Valenzuela, "Torque controller of a doubly-fed induction generator impelled by a DC motor for wind system applications," *IET Renew. Power Generat.*, vol. 8, no. 5, pp. 484–497, 2014.
[23] J. R. Dominguez, C. Mora-Soto, S. Ortega, J. J. Raygoza, and A. De La Mora, "Super-twisting control of induction motors with core loss," in *Proc. 11th Int. Workshop Variable Struct. Syst. (VSS)*, Jun. 2010, pp. 428–433.
[24] H. Wang, P. X. Liu, and P. Shi, "Observer-based fuzzy adaptive output-feedback control of stochastic nonlinear multiple time-delay systems," *IEEE Trans. Cybern.*, vol. 47, no. 9, pp. 2568–2578, Sep. 2017.
[25] H. Wang, P. X. Liu, and B. Niu, "Robust fuzzy adaptive tracking control for nonaffine stochastic nonlinear switching systems," *IEEE Trans. Cybern.*, to be published, doi: 10.1109/TCYB.2017.2740841.
[26] X. Zhao, H. Yang, H. R. Karimi, and Y. Zhu, "Adaptive neural control of MIMO nonstrict-feedback nonlinear systems with time delay," *IEEE Trans. Cybern.*, vol. 46, no. 6, pp. 1337–1349, Jun. 2016.
[27] X. D. Zhao, P. Shi, X. L. Zheng, and J. H. Zhang, "Intelligent tracking control for a class of uncertain high-order nonlinear systems," *IEEE Trans. Neural Netw. Learn. Syst.*, vol. 27, no. 9, pp. 1976–1982, Sep. 2016.

**ONOFRE A. MORFIN** was born in Toluca, Mexico. He received the B.S. degree in electromechanical engineering from the Technological Institute of Toluca, México, in 1990, the M.Sc. degree in electrical engineering from the Monterrey Institute of Technology and Higher Education, Monterrey Campus, México, in 1994, and the Ph. D. degree in electrical engineering from the Advanced Studies and Research Center, National Polytechnic Institute (CINVESTAV_IPN), Guadalajara Campus, Mexico, in 2010. He is currently a Professor with the Departamento de Ingeniería Eléctrica y Computación, Instituto de Ingeniería y Tecnología, Universidad Autónoma de Ciudad Juárez, Chihuahua, Mexico. His research interests include energy saving systems and loop-closed control system designs applied to electrical machines and renewable energy.

**FREDY ALBERTO VALENZUELA** received the M.Sc. degree in electrical engineering from the Graduate Program and Research in Electrical Engineering of the Technological Institute of Morelia, México, in 2006, and the Ph.D. degree in electrical engineering from the Center for Research and Advanced Studies, National Polytechnic Institute, Guadalajara, México, in 2010. He is a member of the state system of CONACYT researcher in the state of Tabasco México. He is currently a Research Professor with the Universidad Juárez Autónoma de Tabasco, Villahermosa, Mexico. His research interests include the analysis and control applied to the control of electrical machines, to alternative energy systems and the efficient use of energy.

**REYMUNDO RAMÍREZ BETANCOUR** received the M.Sc. and the Ph.D. degrees from the Universidad Michoacana, Morelia, México, in 2006 and 2012, respectively. He is currently a Professor in the career of electrical and electronic engineering with the Universidad Juárez Autónoma de Tabasco, Villahermosa, México. His research interests include real-time control systems and power system dynamic analysis.

**CARLOS EDUARDO CASTAÑEDA** received the B.S. degree in communications and electronics from the Universidad de Guadalajara, México, in 1995, the M.Sc. degree in electronics and computer systems from the Universidad la Salle Bajío, México, in 2003, and the Ph.D. degree in electrical engineering from CINVESTAV Guadalajara, México, in 2009. He is a Professor with the Centro Universitario de los Lagos, Universidad de Guadalajara, México. His research interests include automatic control and renewable energy sources.

**RIEMANN RUÍZ-CRUZ** (M'12) was born in Oaxaca, Mexico, in 1983. He received the B.S.E.E. degree from the Instituto Tecnológico de Oaxaca in 2006, and the M.S.E.E. and D.Sc. in electrical engineering from the Advanced Studies and Research Center, National Polytechnic Institute (CINVESTAV-IPN), Guadalajara campus, Mexico, in 2009 and 2013, respectively. Since 2013, he has been with Instituto Tecnológico y de Estudios Superiores de Occidente (ITESO), Guadalajara, Mexico. He is a member of the research group on the Research Laboratory on Optimal Design, Devices, and Advanced Materials (OPTIMA), Department of Mathematics and Physics, ITESO. He is also a member of the Mexican National Research System (Rank 1). His current research interests include neural control, block control, inverse optimal control, and discrete-time sliding modes, and their applications to electrical machines and power systems.

**ANTONIO VALDERRABANO-GONZALEZ** received the B.S. degree in industrial electronics from the Instituto Tecnológico de Puebla, México, the M.Sc. degree in electronics from the Instituto Nacional de Astrofísica, Óptica y Electrónica, México, and the Ph.D. degree in electrical engineering from Cinvestav Guadalajara, México in 2010. He is currently a Professor with Universidad Panamericana Campus, Guadalajara, México. His research interests include power electronics, control of power electronic converters, FACTS devices, and power quality.